Bioprocess and Biosystems Engineering (2024) 47:633–649
https://doi.org/10.1007/s00449-024-02990-w

RESEARCH PAPER

Analyzing of hydrodynamic stress and mass transfer requirements of a fermentation process carried out in a coaxial bioreactor: a scale-up study

Ali Rahimzadeh[1] · **Farhad Ein-Mozaffari**[1] · **Ali Lohi**[1]

Received: 12 December 2023 / Accepted: 4 March 2024 / Published online: 1 April 2024

Abstract

Fluid hydrodynamic stress has a deterministic effect on the morphology of filamentous fungi. Although the coaxial mixer has been recognized as a suitable gas dispersion system for minimizing inhomogeneities within a bioreactor, its performance for achieving enhanced oxygen transfer while operating at a reduced shear environment has not been investigated yet, specifically upon scale-up. Therefore, the influence of the impeller type, aeration rate, and central impeller retrofitting on the efficacy of an abiotic coaxial system containing a shear-thinning fluid was examined. The aim was to assess the hydrodynamic parameters, including stress, mass transfer, bubble size, and gas hold-up, upon conducting a scale-up study. The investigation was conducted through dynamic gassing-in, tomography, and computational fluid dynamics combined with population balance methods. It was observed that the coaxial bioreactor performance was strongly influenced by the agitator type. In addition, coaxial bioreactors are scalable in terms of shear environment and oxygen transfer rate.

Keywords Coaxial bioreactor · Shear environment · Non-Newtonian fluid · Mass transfer

List of symbols

C_0	Oxygen concentration at $t = 0$ (g/L)
n	Power index (-)
C^*	Saturated oxygen concentration (g/L)
N	Impeller rotational speed (1/s)
C_{me}	Oxygen concentration measured by the probe (g/L)
P	Power consumption (W)
Fl_g	Gas flow number (-)
Q	Gas flow rate (vvm)
K	Consistency index (Pa s^n)
t	Time (s)
k_L	Liquid side mass transfer coefficient (m/s)
t_c	Fluid circulation time (s)
k_La	Volumetric mass transfer coefficient (1/s)
V	Liquid volume (m^3)

Greek letters

ε	Turbulent energy dissipation rate (m^2/s^3)
τ_r	Oxygen probe response time (s)
ν	Kinematic viscosity (m^2/s)

Abbreviations

CFD	Computational fluid dynamics
CMC	Carboxyl methylcellulose
DAS	Data acquisition system
EDCF	Energy dissipation/circulation function
ERT	Electrical resistance tomography
PBM	Population balance method
QMOM	Quadrature Method of Moments

Introduction

Foreign gene expression in filamentous fungi as eukaryotic hosts has gained increasing popularity [1]. Their morphology can be classified into two main types of dispersed and pelleted. Characterization of mycelial morphology is essential for the design and scale-up of fungal fermentations. Understanding the relationship between mycelial morphology, oxygen transfer, and overall productivity is critical to effectively optimize the fermentation conditions [2].

✉ Farhad Ein-Mozaffari
fmozaffa@torontomu.ca

1 Department of Chemical Engineering, Toronto Metropolitan University, 350 Victoria Street, Toronto, ON M5B 2K3, Canada

The performance of stirred tank bioreactors, including cell metabolism and viability, is susceptible to the shear sensitivity of the cell culture medium. The elevated agitation intensity can lead to shear damage, reducing the efficacy of the fermentation process [3]. Nienow [4] suggested using the term “fluid dynamic stresses” instead of “shear” to describe the effect of the mixing hydrodynamics on cells within the bioreactor. Currently, there is ongoing debate regarding the influence of hydrodynamic stress on fermenter performance. For instance, animal cell cultures are often considered shear sensitive, because they do not possess a protective cell wall [3, 5, 6]. Consequently, bioreactors containing animal cells typically operate under suboptimal conditions, leading to significant inhomogeneities that act as a barrier to successful scale-up [7, 8]. On the other hand, some studies showed that the agitation intensity has no impact on the production of protein therapeutics, with the exception of mycelial broth, such as filamentous fungal cell cultures [4]. In fact, when the shear stress is stronger than the tensile strength of a hyphae, cell fragmentation happens [9]. Therefore, the impact of agitation-induced hydrodynamic stress on cell cultures varies depending on the cell type [10].

The growth of filamentous organisms can give rise to large and complex shapes, leading to the production of viscous, rheologically complex broths [11, 12]. Because of that, high agitation intensity is often necessary to meet the mass transfer requirements of the fermentation process. However, excessive agitation can result in morphological changes and hyphal fragmentations, which may adversely affect product expression [13]. As a result, agitation intensity in fungal fermentations is carefully adjusted to provide suitable oxygen transfer and mixing while preventing adverse effects on the microorganisms. Among various methods for quantifying fluid dynamic stresses, only the energy dissipation/circulation function (EDCF) has shown strong correlation with the morphology of the fermentation broth [14]. This function establishes a connection between the frequency at which mycelial pass through the impeller's swept volume and the rate of specific energy dissipation within that region [2].

In spite of the influence of agitation intensity and high EDCF values on mycelial morphology, some authors have raised questions regarding the direct influence of mycelial shape on fermentation productivity [1, 13]. Nienow [15] stated that an increased EDCF value results in reduced clump size and lower viscosity due to hyphae fragmentation. Indeed, the lower viscosity resulting from the increased EDCF value enhances mass transfer and homogeneities in the system. While the impact of high EDCF values on the productivity of filamentous fungi remains a subject of controversy, existing literature unanimously agrees that altering EDCF values can lead to changes in the shape and size of fungal clumps. On the other hand, mycelial morphology plays a critical role in determining fermentation performance, encompassing aspects, such as mass transfer, fluid viscosity, and mixing hydrodynamics [2]. As a result, based on our literature review, EDCF is one of the most crucial bioreactor characteristics that must be considered in fermenter design and scale-up.

Bioreactor scale-up introduces significant changes in the microorganism environment. Achieving a good mixing at larger scales can be challenging, leading to the formation of dissolved oxygen heterogeneities in aerobic fermenters [16, 17]. Such heterogeneities, commonly observed in poorly mixed large-scale bioreactors, can have substantial impacts on cells [18, 19]. The characteristics of these heterogeneities depend on factors such as fluid dynamics and nutrient dispersion [20]. In fact, homogeneity becomes increasingly important at large scales [21] and heterogeneities within the bioreactor can result in various metabolic responses and production of undesired byproducts [5, 22]. In addition, filamentous fungal fermentations pose particular difficulties in scale-up due to the complex rheology of the broth, significantly affecting mass transfer rate [13, 23].

Nowadays, mixing system retrofitting has emerged as a crucial practice to reduce process costs and enhance mixing efficiency, specifically during the scale-up process. Due to the rise in popularity of mixing system retrofitting caused by the development of single-use bioreactors [3, 24], careful consideration is required while switching to such bioreactors [7]. Retrofitting offers numerous advantages, including the reduction of mechanical instabilities and vibrations in the mixing system, minimizing shear rates, and enhancing mass transfer capabilities. Among the prevailing and easily implemented retrofitting approaches, changing the impeller type stands out as one of the most common methods. By selecting a suitable impeller type, the performance and functionality of the mixing system can be significantly improved [2, 25, 26].

Generally, impellers can be classified into two main types of the axial-flow and radial-flow impellers. Radial-flow impellers are characterized by their flow direction perpendicular to the impeller shaft. The Rushton turbine as a radial-flow impeller generates a staged-flow pattern with a well-mixed zone near the impeller's blade [26]. On the other hand, the axial-flow impellers have a flow direction parallel to the impeller shaft, offering improved top-to-bottom blending. Consequently, using a lower power number impeller that possesses good air handling capabilities instead of a higher power number impeller allows for cost effective retrofitting [26]. Moreover, impellers can be categorized as either low shear or high shear. It has been suggested that low shear impellers may cause less damage to filamentous organisms compared to high shear impellers when operated at similar specific power [27]. Nevertheless, further investigations have revealed that this presumption is not accurate. In fact, so-called low shear impellers can possess high-energy dissipation/circulation function (EDCF) values [28].

Recently, computational fluid dynamics (CFD) has emerged as a highly promising method for studying shear rate and transport phenomena occurring within bioreactors [29–32]. The adoption of CFD tool for defining a design space has gained popularity in pharmaceutical applications, offering assurance of product quality. CFD simulations can predict optimum mixing in bioreactors, proposing a design space that ensures consistent quality. By employing the CFD method, the impact of hydrodynamic stress, fluid flow patterns, and gas dispersion uniformity can be optimized. Deviations from this defined design space are considered changes and may trigger a regulatory post approval change process in pharmaceutical industry [33].

In addition to radial-flow and axial-flow impellers, there is another specific type known as tangential-flow impellers. These impellers are suitable for the bulk movement of a highly viscous fluid within a bioreactor. It has been demonstrated that the simultaneous use of a tangential-flow impeller, such as an anchor impeller, in conjunction with a central impeller (either axial-flow or radial-flow) can significantly improve the homogeneity of gas dispersion inside the bioreactor [34, 35]. This combined system, known as a coaxial bioreactor, enhances the mixing process while requiring a lower power input. The combined effect of both anchor and central impellers in a coaxial bioreactor leads to improved hydrodynamics and enhanced mixing efficiency [36–38].

The use of model fluids has become a common practice to replicate the viscous fermentation broth from a rheological perspective [39–41]. This approach allows for ease of operation and consistency in experimental conditions across different batches and experiments. For filamentous fungi fermentation, abiotic systems can mimic the fermentation broth using a non-Newtonian model solution [42] that exhibits shear-thinning behavior [43–45]. A comprehensive review of the literature highlights the importance of EDCF in the design and scale-up of filamentous fungus fermentation. The highly oxygen-demanding nature and complex rheology of the fermentation process make scale-up studies even more intricate. Consideration of the interplay between oxygen transfer and mechanical stress is crucial in optimizing and scaling up the bioreactor [25, 46]. However, there is a lack of published data addressing the effect of the shear environment and mass transfer rate inside a coaxial bioreactor containing a shear-thinning fluid, especially during the scale-up process. Coaxial mixers are recognized for their enhanced mass transfer coefficients at lower aeration rates. Therefore, this study focused on lower aeration values compared to those typically used in large-scale aerobic fermentations in industries.

The aim of this investigation was to assess the hydrodynamic stress and central impeller retrofitting influence on the performance of an abiotic system using a coaxial bioreactor during the scale-up process. To achieve this objective, we examined the effects of impeller type, aeration rate, and agitation rate on shear environment, mass transfer rate, bubble size distribution, and spatial inhomogeneities. The findings of this study hold significant value in optimizing the design, scale-up, and operation of fungal fermentations.

Materials and methods

Experimental setup

Two flat-bottomed cylindrical bioreactors were fabricated. Air was introduced inside the vessel through a ring gas distributor. The liquid height inside the bioreactor was equal to the vessel diameter. A schematic diagram and dimensions of both apparatuses are shown in Fig. 1. Each mixing system was furnished with a central impeller and an anchor impeller mounted on two separate shafts. Both the anchor and central impeller were rotating in the same direction (co-rotating mode). The working volume of the small-scale and large-scale tanks were about 50 and 173 L, respectively. In this paper, a coaxial bioreactor furnished with a central impeller of an elephant ear, a Scaba, a pitched blade, and a Rushton turbine was used. It should be noted that all axial-flow impellers employed in this study functioned in up pumping flow mode.

Abiotic system

Instead of the fermentation broth, a suitable alternative is simulated medium that replicates the desired rheological characteristics to mimic the viscosity, shear rate, and other relevant rheological properties of the actual fermentation broth. Therefore, a model fluid exhibiting shear-thinning behavior was selected. The rheological properties of filamentous fungus fermentation broths are influenced by the formation of clumps or aggregates within the broth. As a consequence, the rheological behavior of these fermentation broths can encompass a diverse range of shear-thinning behavior. Hence, in this study, 0.5 wt% NaCMC (sodium carboxymethyl cellulose) solution was used as an abiotic system. The rheological properties of the liquid phase were analyzed using the Bohlin C-VOR Rheometer 150 (Malvern Instruments, UK) at 22 ± 1°C. It was found that the working fluid follows power-law non-Newtonian model with the power law of 0.65, and consistency index of 2.36 Pa s^n.

The fluid density was 0.965 kg/m^3 and the kinematic diffusion was approximately 1.71 e -9 m^2/s [36]. Furthermore, the gas phase was the air at 22 ± 1°C.

Fig. 1 Experimental setup

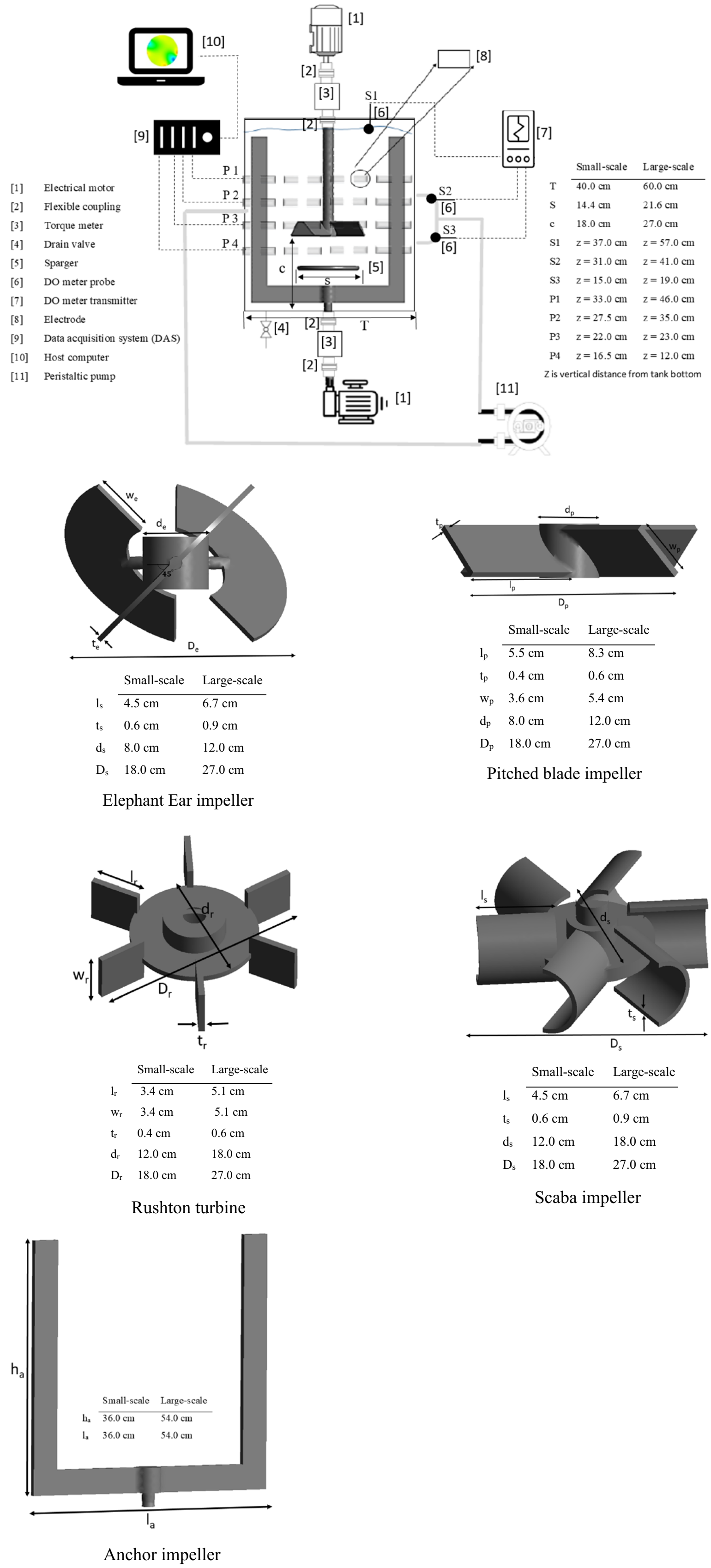

Power consumption

The total power consumption resulted from the combined power consumed by both the central impeller and the anchor. Therefore, in this research, the torque generated by each impeller was individually assessed using dedicated torque meters from S. Himmelstein Company (USA). Subsequently, the obtained torque measurements were adjusted by subtracting any residual torques attributable to friction. The net power consumption of each impeller was calculated using the following equation:

$$P = 2\pi NM, \tag{1}$$

where M and N are the net torque and the impeller rotational speed, respectively.

Gas hold-up

To measure the gas phase retention within the mixing vessel, the electrical resistance tomography (ERT) method was applied. Each bioreactor was furnished with four sensor planes at different heights. Each plane was comprised of 16 stainless steel electrodes with a rectangular shape. The height of sensor planes and electrode dimensions are illustrated in Fig. 1. In this technique, the conductivity profile of the multiphase mixture was measured by an ERT system. By utilizing the simplified Maxwell equation, the obtained conductivity profile was converted to a gas phase volume fraction [38]. Hence, the gas hold-up distribution was obtained.

Mass transfer coefficient ($k_L a$)

The dynamic gassing-in method was employed to determine the volumetric mass transfer coefficient ($k_L a$). In this method, the oxygen was stripped out of the filled mixing tank via aeration with nitrogen. Then, oxygen was introduced, and the oxygen concentration was recorded until the upper dissolved oxygen (DO) probe reached to its 90% of saturation condition.$k_L a$ was determined by employing the following equation [41]:

$$C_{me} = C^* + \frac{C^* - C_0}{1 - \tau_r k_\mathrm{L} a}\left[\tau_r k_\mathrm{L} a \exp\left(-\frac{t}{\tau_r}\right) - \exp(k_\mathrm{L} a.t)\right], \tag{2}$$

where C_{me}, C^*, C_0 are oxygen concentration measured by the probe, oxygen concentration at saturation condition, and initial oxygen concentration, respectively. In addition, τ_r is the probe response. As shown in Fig. 1, each bioreactor was equipped with three different DO probes at various heights. The response time for Probe #1 was 49 s and for two other probes was 20 s. The overall mass transfer coefficient was calculated as the arithmetic mean of the results attained from each individual oxygen probe.

Computational fluid dynamics (CFD)

In this study, the abiotic system inside the coaxial bioreactor was modeled using the Eulerian–Eulerian multiphase approach. The turbulence within the coaxial bioreactor was simulated using a standard k-ε model, complemented by an enhanced wall treatment function to improve accuracy near the boundaries. The enhanced wall treatment method combines the advantages of standard wall treatments for low *Re* numbers near the wall with wall functions for approximating the wall's effect on fluid flow near the wall for high *Re* numbers. The bubble-induced turbulence viscosity was considered using the Sato and Sekoguchi model [47]. The modified drag model proposed by Brucato et al. [48] was used to couple the gas and liquid momentum balance equations.

Population balance method (PBM)

To address the variation in air bubble sizes within the bioreactor, the population balance equation (PBE) was incorporated into the model via utilizing the quadrature method of moments (QMOM) approach. The QMOM method involved tracking six moments to accurately represent the distribution of bubble sizes [37]. This method stands out for its efficiency in terms of computational resources compared to other PBE-solving techniques. To simulate bubble breakage phenomena, the kernel introduced by Laakkonen et al. [49] was utilized, enabling a realistic representation of the breakage process. For bubble coalescence, the model suggested by Luo [50] was utilized.

Mass transfer coefficient and EDCF model

The liquid-side mass transfer coefficient was determined using the penetration model proposed by Higbie [51]

$$k_L = \frac{2}{\sqrt{\pi}}\sqrt{D_L}\left(\frac{\varepsilon}{\upsilon}\right)^{1/4}; \tag{3}$$

in this model, ε is the turbulent energy dissipation rate, D_L corresponds the kinematic diffusion coefficient, and υ refers liquid kinematic viscosity.

This study employed a method to quantify the shear environment by integrating the turbulence dissipation rate with the frequency of mycelium exposure to the high shear zone, leading to the establishment of the energy dissipation/circulation function (EDCF). The energy dissipation rate was calculated based on the volume averaged turbulence energy dissipation rate acquired from the CFD simulations within the central impeller swept volume. The frequency of the mycelium exposure or break-up frequency is $1/t_c$. Here, t_c is the circulation time and was calculated as follows [14]:

$$t_c = \frac{V}{Fl_g ND^3}; \quad (4)$$

in this equation, V represents the bioreactor volume. N and D correspond to the rotational speed and diameter of the central impeller, respectively. In addition, Fl_g is the gas flow number of the central impeller indicating its pumping capability

$$Fl_g = \frac{q}{ND^3}; \quad (5)$$

in this equation, q is the fluid flow rate discharged from the central impeller swept volume and it was determined from the results obtained from the CFD simulations [52].

CFD solver

A commercial CFD package (ANSYS FLUENT 2022 R2) was used. The QUICK and the second-order upwind techniques were employed to discretize the volume fraction and momentum, respectively. The tetrahedral mesh was applied to model the mixing system geometry. The boundary conditions used in this study are provided in Fig. 2. It should be noted that no slip boundary condition is valid for both gas and liquid phases. In addition, the sliding mesh method was used to model the all moving zones [53].

In this study, the minimum and maximum bubble size were set to 1 and 100 mm, respectively. The Miller [54] model was used to predict the bubble size on the sparger

$$d_b = \left(\frac{6\sigma d_0}{g(\rho_l - \rho_g)} \right)^{\frac{1}{3}}, \quad (5)$$

where d_0 is the diameters of the holes in the sparger, and σ is the surface tension of the fluid.

Simulations were conducted with a time step of 0.001 s. The SIMPLE algorithm was applied to perform the pressure–velocity coupling. The CFD simulations were solved for a minimum of 50 rotations of the central impeller. Also, a 120 partitioned parallel solver was applied to perform the simulations, utilizing the computational resources available in the Niagara Supercomputing Facilities. Each simulation required about 24 h of clock time.

Mesh independence test and model validation

To determine the most suitable mesh size, a test for grid-independence was conducted. Three distinct mesh sizes were developed for the large-scale bioreactor model with 2,224,953, 4,673,962, and 6,228,801 cells. A comparison between the results obtained from the second and third mesh sizes revealed that the difference in volume average velocity at the impeller region for the large-scale Pitched blade-anchor mixer operating at 200 rpm was less than 2.5%. Additionally, the disparity in global gas hold-up obtained through CFD was below 6.3 percent. Considering the computational efficiency in terms of computational cost, the CFD model

Fig. 2 Boundary conditions of the numerical model

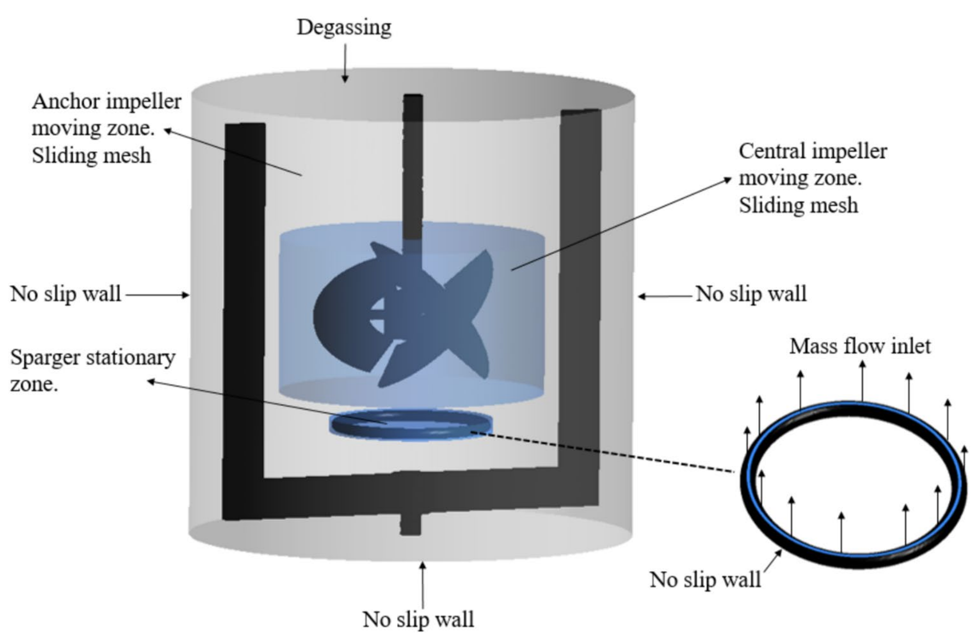

Fig. 3 Computational grid

Table 1 Comparison of the measured and calculated gas hold-up of the Elephant ear-anchor bioreactor (an anchor impeller speed of 10 rpm, a central impeller speed of 400 rpm, an aeration rate of 0.12 *vvm*, and 0.5 wt% NaCMC)

Plane number	EXP	CFD
1	0.0092	0.0088
2	0.0016	0.0166
3	0.0234	0.0228
4	0.0182	0.0190

with 4,673,962 cells was selected for the large-scale mixer. Furthermore, the grid-independence test for the small-scale bioreactor indicated that 1,673,962 cells were sufficient for simulations with adequate precision. The computational grid is shown in Fig. 3.

The accuracy of CFD simulations was checked using the spatial gas hold-up findings. As indicated in Table 1, the results obtained from the CFD model demonstrated reasonable agreement with the experimental data.

Results and discussion

Hydrodynamic stress and mass transfer

It is important to investigate the performance of the gas dispersion system under different operating conditions while maintaining a consistent specific power consumption. To achieve this objective, the specific power consumption of the small-scale coaxial bioreactor remained constant at 1.2 kW/m^3 for all operating conditions and bioreactor configurations. This was due to the fact that most agitated bioreactors containing filamentous fungi are operated under similar specific power consumption [10]. It is crucial to note that increasing the aeration rate (Q) leads to a reduction in aerated power consumption at a constant impeller speed. To prevent such a reduction in aerated power consumption during aeration, the central impeller speed (N_c) was increased by increasing the aeration rate. In fact, by increasing N_c, the negative effect of the aeration rate on the total aerated power consumption obtained by the small-scale bioreactor was eliminated. Because of that, all the data reported in Fig. 4 were obtained at the same aerated power consumption. To achieve this objective, the specific power consumption of the small-scale coaxial bioreactor remained constant at 1.2 kW/m^3 for all operating conditions and bioreactor configurations. In this regard, the aeration rates and central impeller speeds used for the small-scale coaxial bioreactor are listed in Table 2.

The shear environment obtained by the small-scale bioreactor as a function of the aeration rate is presented in Fig. 4. As shown in this figure, by increasing Q, the shear environment created inside the bioreactor increased for all coaxial bioreactor configurations. Because by increasing Q, the total turbulence intensity generated inside the bioreactor was increased. In fact, as per the discussion in "Mass transfer coefficient and EDCF model" section, the EDCF has a direct relationship with turbulence intensity. Increasing both the impeller speed and aeration rate increased the energy dissipation rate, and as a result, the mixing fluid encountered higher shear rates. Moreover, increasing the aeration rate enhanced k_La obtained by the coaxial mixer. k_La comprises the liquid-side mass transfer coefficient and the interfacial area. The liquid-side mass transfer coefficient increased by increasing the level of turbulence intensity, and on the other hand, the interfacial area is function of the gas hold-up. Since gas hold-up increased by increasing the aeration rate in this study, the k_La obtained by the small-scale mixer improved by increasing the aeration rate.

The results attained by the coaxial bioreactor furnished with an axial-flow central impeller are shown in Fig. 4a and b. It was observed that the overall EDCF values acquired with the Pitched blade-anchor mixer exceeded those achieved with the Elephant ear-anchor bioreactor. Meanwhile, the Pitched blade-anchor bioreactor exhibited greater k_La compared to the Elephant ear-anchor bioreactor.

As can be noted in Fig. 4c and d for the coaxial bioreactor equipped with a radial-flow central impeller, the shear environment achieved with the Rushton turbine-anchor bioreactor was more intense than those attained with the Scaba-anchor bioreactor. In contrast, the Scaba-anchor bioreactor

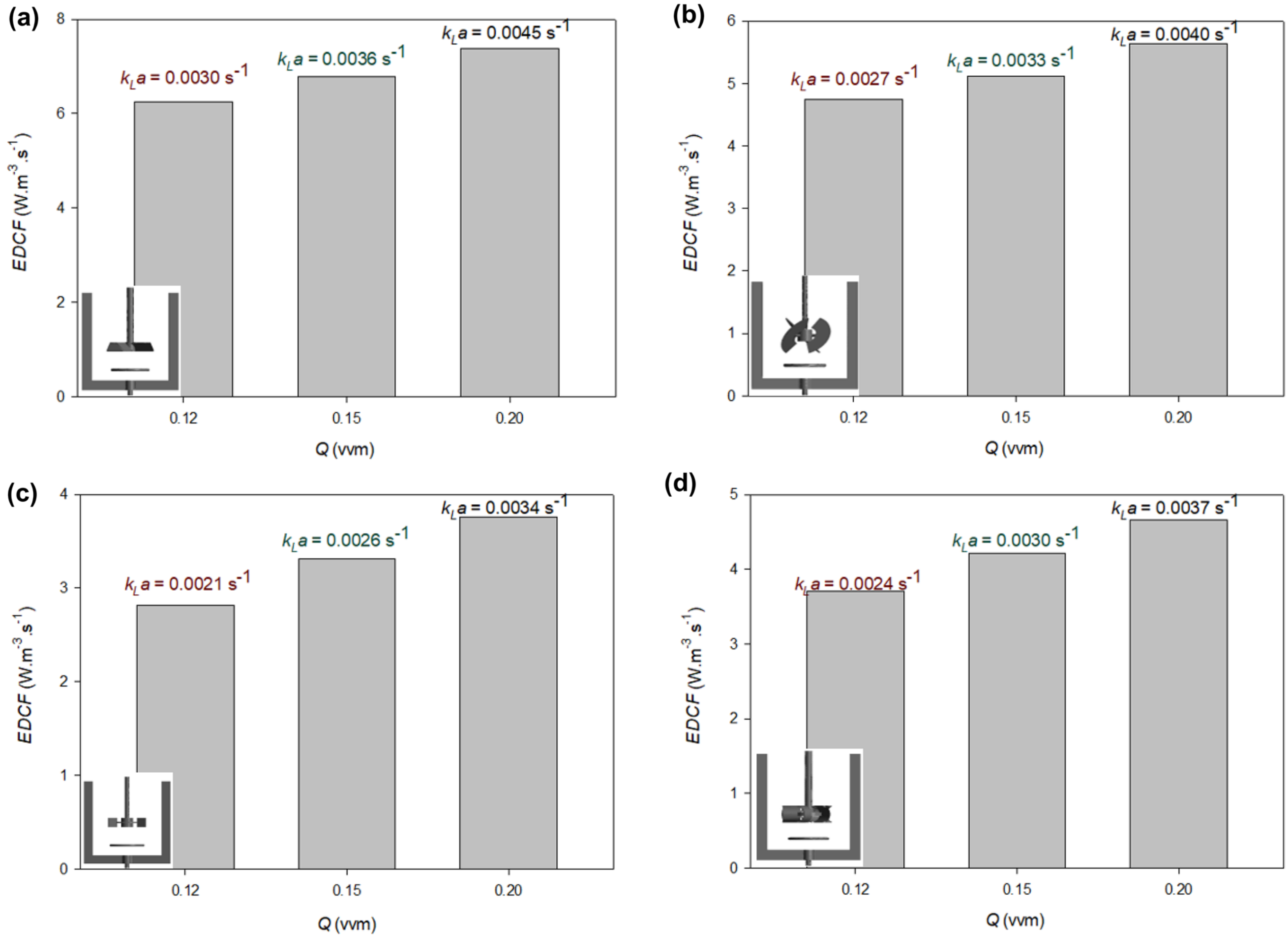

Fig. 4 Shear environment and k_La of the small-scale coaxial bioreactor as a function of the aeration rate: **a** Pitched blade-anchor, **b** Elephant ear-anchor, **c** Rushton turbine-anchor, and **d** Scaba-anchor (the deviation for k_La was less than ± 1.54%)

Table 2 Operating conditions for the small-scale coaxial bioreactor

Configuration	Aeration rate (vvm)			Anchor impeller speed (rpm)
	0.12	0.15	0.20	
	Central impeller speed (rpm)			
PBU-anchor	400	450	500	10
EE-anchor	440	480	540	
RT-anchor	315	360	410	
Sc-anchor	290	375	400	

demonstrated a higher mass transfer coefficient. This observation suggests that the Scaba-anchor mixer's efficiency surpasses that of the Rushton turbine-anchor bioreactor. Because, for the Scaba-anchor bioreactor, a higher k_La was achieved at the reduced shear environment.

Upon a comparison of the outcomes illustrated in Fig. 4a and b with those presented in Fig. 4c and d, it became evident that the shear environment established by the coaxial bioreactor featuring a radial-flow impeller was less intense than those achieved by the axial-flow impeller. Additionally, the axial-flow impeller exhibited a superior mass transfer coefficient when contrasted with the radial-flow impeller. The effect of the impeller type on the shear environment and k_La will be discussed in detail later in this paper.

The gas hold-up profile inside the bioreactor equipped with either a radial-flow or an axial-flow central impeller was investigated by both numerical and experimental methods. For the Scaba-anchor mixer, by increasing Q from 0.12 to 0.15 vvm, there was a noticeable augmentation in the gas hold-up profile (Fig. 5a and b). The conductivity profiles obtained from the ERT technique are illustrated in Fig. 5c and d. By adding the gas phase inside the bioreactor, the conductivity of the abiotic system decreased. Therefore, areas characterized by lower conductivity correspond to regions with higher gas retention. As presented in these figures, the gas hold-up uniformity acquired by the Scaba-anchor mixer at $Q = 0.15$ vvm was significantly better than that attained at a lower aeration rate. In fact, the conductivity profile

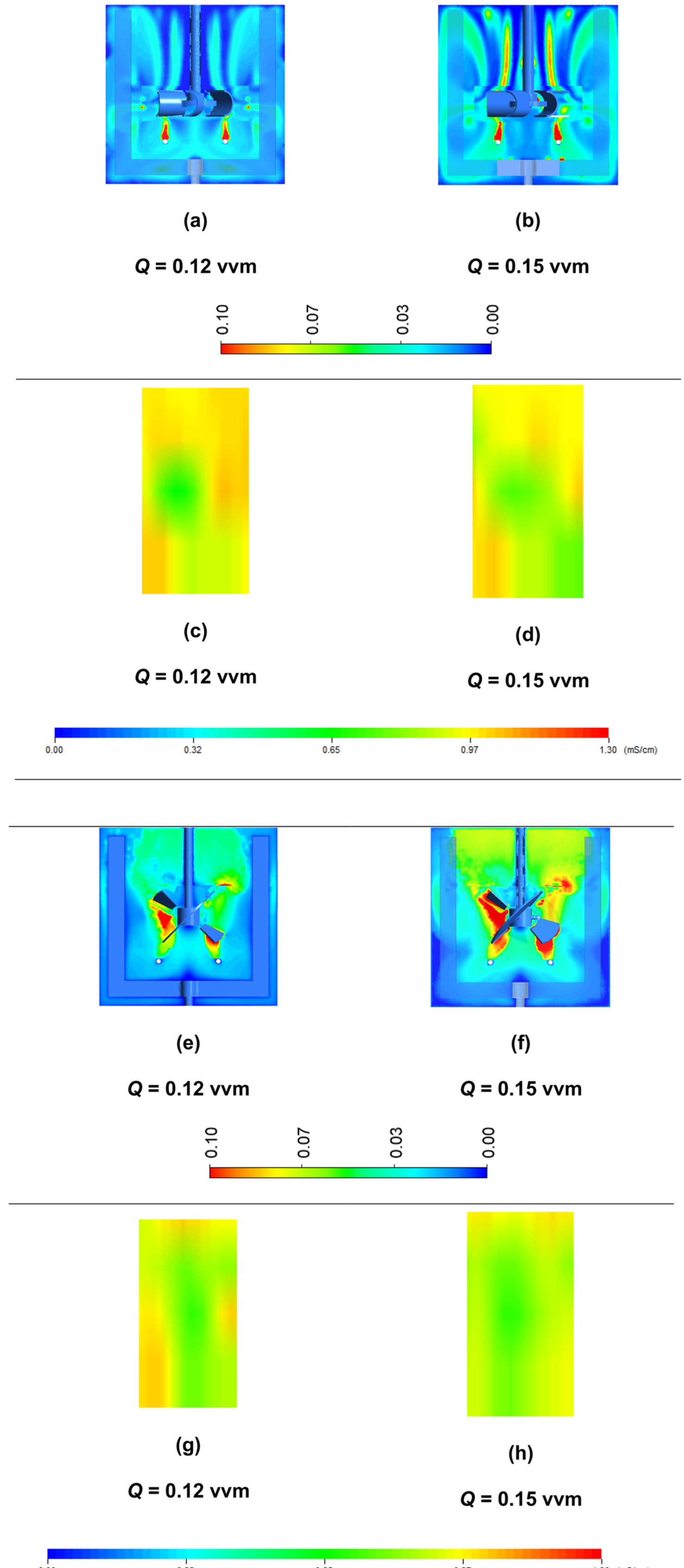

Fig. 5 Gas hold-up profile of the small-scale coaxial bioreactor determined using both CFD and ERT methods: **a**, **b**, **c**, and **d** Scaba-anchor, **e**, **f**, **g**, and **h** Elephant ear-anchor

obtained from the ERT method showed that by increasing Q, the air was dispersed more evenly within the bioreactor. This finding holds particular significance for highly oxygen-demanding microorganisms. Furthermore, the gas hold-up detected in the region surrounding the central impeller was higher than that observed elsewhere within the bioreactor. Hence, the majority of oxygen transfer took place in the vicinity of the central impeller region.

For the bioreactor equipped with the elephant ear central impeller as an axial-flow impeller, almost similar behavior was observed as a Scaba-anchor mixer. However, the Elephant ear-anchor bioreactor generated a greater gas hold-up compared to the Scaba-anchor bioreactor when operating at the identical aeration rates and specific power consumption. This observation confirmed the findings presented in Fig. 4, which showed the superior $k_L a$ of the Elephant ear-anchor mixer. Indeed, the primary factor contributing to the higher mass transfer coefficient in these bioreactors, as opposed to those equipped with a radial-flow central impeller, was the greater gas hold-up achieved by the axial-flow impeller.

Importantly, by comparing the results depicted in Fig. 5g and h with those depicted in Fig. 5c and d, it was concluded that the gas hold-up homogeneity achieved with the Elephant ear-anchor bioreactor was significantly better than that accomplished with the Scaba-anchor bioreactor. Therefore, the microorganisms inside the coaxial bioreactor with an axial-flow impeller would encounter a uniform environment within the bioreactor.

Scale-up with complete geometrical similarity

In this section, the scale-up study was carried out with complete geometrical similarity. The scale-up was executed utilizing the constant $k_L a$ approach, which ensured the preservation of the mass transfer coefficient at the same level as that observed in the small-scale bioreactor, for the large-scale counterpart. To preserve $k_L a$ of the large-scale bioreactor at the same level as its small-scale counterpart under similar aeration rates per working fluid volume, the central impeller agitation rate was increased. The operating conditions of the large-scale system upon scale-up is reported in Table 3.

Table 3 Operating conditions for the large-scale coaxial bioreactor

Configuration	Aeration rate (vvm)			Anchor impeller speed (rpm)
	0.12	0.15	0.20	
	Central impeller speed (rpm)			
PBU-anchor	440	500	550	
EE-anchor	490	530	600	10
RT-anchor	360	410	470	
Sc-anchor	330	400	440	

The shear environment obtained by the bioreactor at various scales and operating conditions is presented in Fig. 6. It was observed that for all bioreactor configurations whether equipped with an axial-flow or radial-flow impeller, the EDCF value achieved by the large-scale bioreactor exceeded that obtained by the small-scale. Indeed, for the large-scale bioreactor, the energy dissipation rate in the central impeller swept volume was increased to improve $k_L a$ during the scale-up with complete geometrical similarity. In other words, the key factor behind the increased shear environment in the large-scale bioreactor, in contrast to its small-scale counterpart, was primarily the heightened turbulence energy dissipation rate.

Upon conducting the scale-up, the change in EDCF value achieved at a low aeration rate was minimal. However, at $Q = 0.20$ vvm, the EDCF value obtained by the large-scale bioreactor was considerably higher than that acquired by its small-scale counterpart. This was attributed to the necessity of significantly increasing the agitation rate of the large-scale system to enhance $k_L a$ when the aeration rate was raised.

To further elaborate on this finding, the specific power consumption (power consumption per working fluid volume) obtained by the large-scale bioreactor was examined, as shown in Fig. 6b. It was found that for the scale-up at a constant mass transfer coefficient method and with geometrical similarity, the specific power consumption of the large-scale bioreactor was lower than that of its small-scale counterpart. This difference could be attributed to the larger cavity size generated near the central impeller region in the large-scale bioreactor. As a result, the homogeneity of the mixing system decreased upon scale-up. Moreover, it can be observed that the amount of specific power consumption at a higher aeration rate was less than that discovered at a lower aeration rate. The detailed explanation for this phenomenon has been extensively discussed in the literature before [37]. To attain an equivalent level of specific power consumption (P/V) as the large-scale mixer, the total power consumption (P) had to be three times greater than that of the small-scale counterpart, because the working fluid volume of the large-scale bioreactor was three times greater than that of the small-scale. Indeed, during the scale-up process, despite an increase in power consumption and energy dissipation rate within the central impeller swept volume, the specific power consumption was reduced. This result was achieved by adopting a constant mass transfer approach and maintaining geometrical similarity between the small and large-scale setups.

The shear environment inside a bioreactor directly depends on the turbulent energy dissipation rate and hydrodynamic intensity. The turbulence energy dissipation rate and fluid flow pattern attained by the coaxial bioreactor are

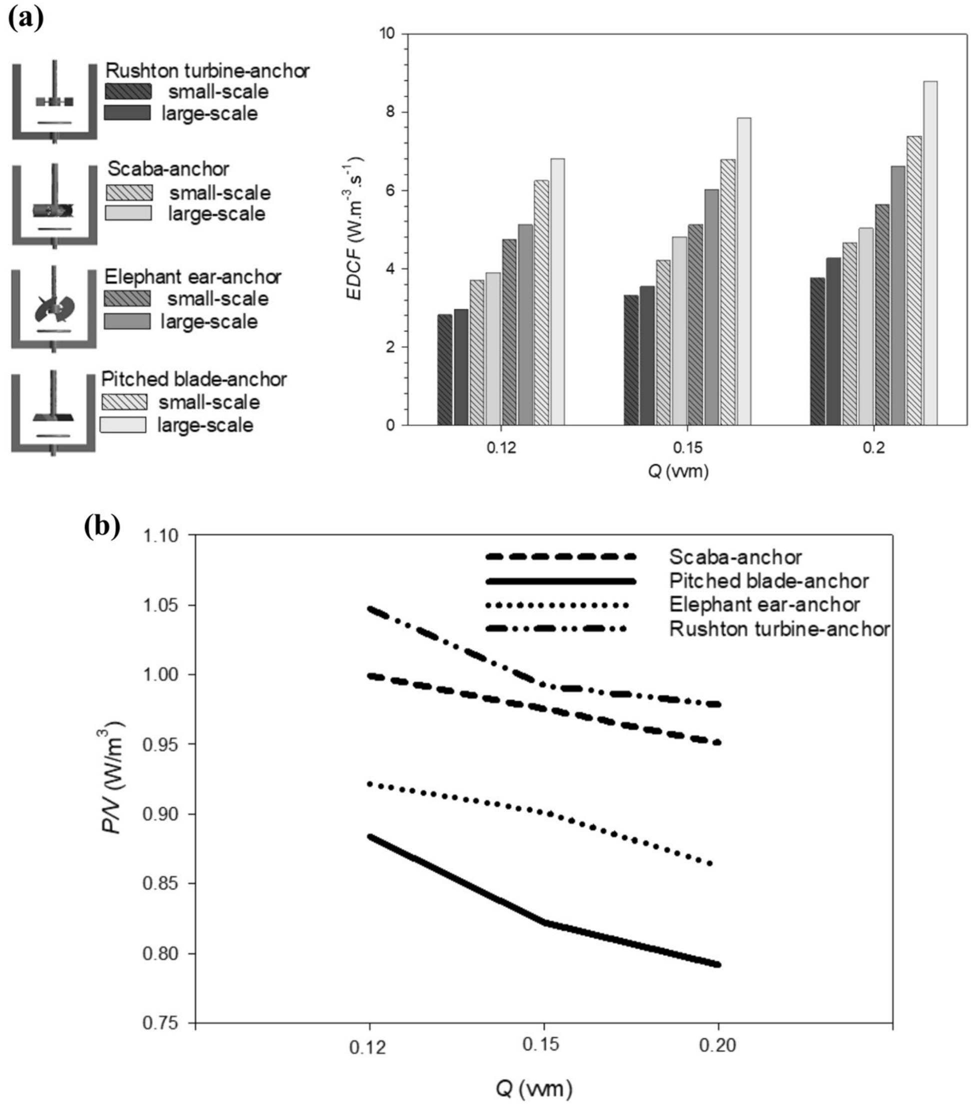

Fig. 6 Specific power consumption and shear environment in coaxial bioreactors at various aeration rates during scale-up, without retrofitting of the central impeller: **a** EDCF and **b** specific power consumption

shown in Fig. 7. As discussed per the results illustrated in Fig. 6, for the large-scale bioreactor, the energy dissipation rate observed in the impeller swept volume was greater than that detected for the small-scale. As depicted in Fig. 7a and b, the CFD simulation results also validated this finding. Moreover, according to the CFD simulation results, the fluid flow pattern demonstrated that the fluid discharged from the central impeller blade of the large-scale bioreactor was considerably more intense than that of the small-scale bioreactor profiles for both bioreactors, equipped with either a radial-flow impeller or an axial-flow impeller.

Scale-up with central impeller retrofitting

In this section, the investigation focused on examining the influence of the central impeller type during the scale-up process of a coaxial bioreactor. In this study, the performance of different types of central impellers, including the radial-flow and the axial-flow impeller, was separately assessed to ensure a comprehensive and adequate comparison. As a matter of fact, a small-scale Rushton turbine-anchor bioreactor was retrofitted with a Scaba-anchor bioreactor. Under these circumstances, both bioreactors were equipped with a radial-flow central impeller. Likewise, for the bioreactor with an axial-flow central impeller, the Pitched blade-anchor mixer was retrofitted with an Elephant ear-anchor mixer upon conducting the scale-up study based on the constant k_La method.

EDCF as a function of aeration rate for the scale-up of a coaxial bioreactor is presented in Fig. 8. Interestingly, it was observed that the shear environment obtained by the large-scale bioreactor was almost the same as that attained by the small-scale bioreactor upon scale-up. Moreover, it was observed that, for both radial-flow and axial-flow bioreactors, the shear environment of the large-scale

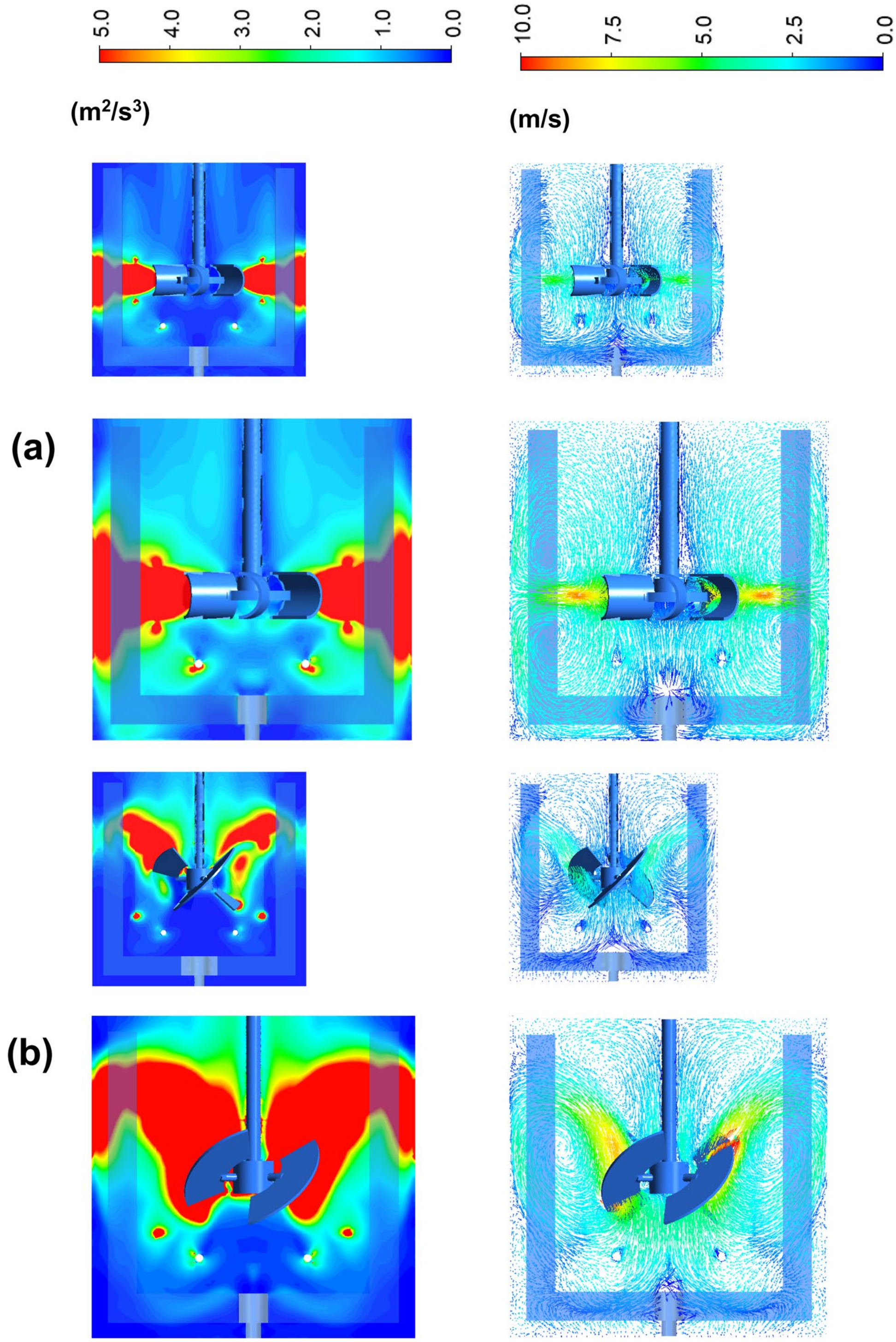

Fig. 7 CFD outcomes pertaining to the fluid velocity vector and the rate of energy dissipation in the coaxial bioreactor during the scale-up process: **a** Scaba-anchor, $Q = 0.12$ vvm, and **b** Elephant ear-anchor $Q = 0.15$ vvm

bioreactor was a little lower than that of the small-scale bioreactor upon the central impeller retrofitting.

As previously discussed in "Introduction" section, the morphology of filamentous fungi is well correlated with the EDCF value. Consequently, it is crucial to accurately predict and maintain the EDCF value during the scale-up process to ensure consistent results. Under these circumstances, fluid rheological behavior, mass transfer requirements, and hydrodynamic stress can be adjusted before conducting a scale-up experiment.

To further elaborate on the influence of the central impeller retrofitting on the shear environment generated by the large-scale bioreactor, the results obtained from the CFD simulations are provided in Fig. 9. The rate of energy

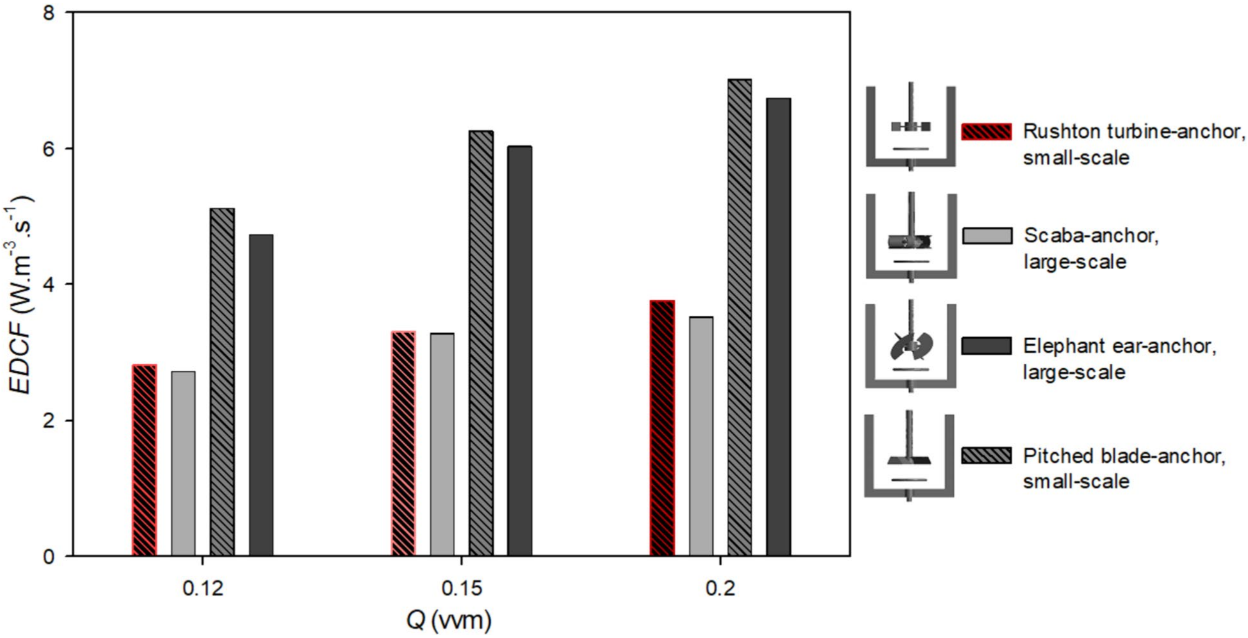

Fig. 8 Shear environment in coaxial bioreactors at various aeration rates during scale-up with retrofitting of the central impeller

dissipation near the central impeller blades was higher. However, the amount of energy dissipation rate obtained by the large-scale bioreactor was almost the same as that gained by the small-scale bioreactor. As delineated in Fig. 9a and b, by changing the central impeller type from the Pitched blade impeller to the Elephant ear impeller, mixing uniformity considerably increased. Furthermore, the fluid flow pattern generated by the Elephant ear-anchor bioreactor demonstrated better top-to-bottom blending compared to that created by the Pitched blade-anchor bioreactor. This can be attributed to the high pumping capacity of the elephant ear impeller compared to that of the Pitched blade impeller. A similar trend was also observed during the scale-up of the radial-flow bioreactor when the central impeller was retrofitted from a Rushton turbine to the Scaba impeller. These findings illustrated the significance of the appropriate impeller selection during the scale-up of a bioreactor containing a shear-thinning fluid.

The question may arise as to how a scale-up with a lower EDCF resulted in an improved mass transfer coefficient. To address this question, the mass transfer profile and air mean bubble diameter were investigated and are presented in Fig. 10 for the scale-up of a coaxial bioreactor with central impeller retrofitting. The observation clearly indicated that k_La obtained by the large-scale bioreactor was not only higher than that achieved by the small-scale bioreactor but also that the uniformity of the mass transfer profile was significantly improved. In fact, the hydrodynamic inhomogeneity was reduced for the scale-up with central impeller retrofitting. This was also confirmed as per the results depicted in Fig. 9. Therefore, the energy dissipated by the central impeller inside the abiotic system was uniformly distributed throughout the bioreactor. Figure 10 shows that the mean diameter of air bubbles achieved through the operation of the large-scale bioreactor was smaller in comparison to the outcomes observed with the small-scale bioreactor. Consequently, this difference in the bubble size led to a greater interfacial area being generated by the large-scale bioreactor, thereby resulting in a higher level of mass transfer when compared to the performance of the smaller scale bioreactor. The small bubble size achieved by the large-scale bioreactor was attributed to the effective hydrodynamics generated by the coaxial bioreactor, which successfully broke down the air into smaller sizes. Therefore, by retrofitting the central impeller of the large-scale coaxial bioreactor upon conducting a scale-up study based on the constant mass transfer technique, both oxygen transfer homogeneity and shear environment were enhanced. The low shear environment and enhanced oxygen transfer can provide a gentle gas dispersion environment for the filamentous fungus cell culture.

Conclusion

This study investigated the performance and scalability of a coaxial bioreactor for filamentous fungus cell culture, focusing on fluid dynamics aspects. The system was successfully scaled up using central impeller retrofitting with both radial-flow and axial-flow impellers. Our findings revealed that the radial-flow impeller exhibited a lower

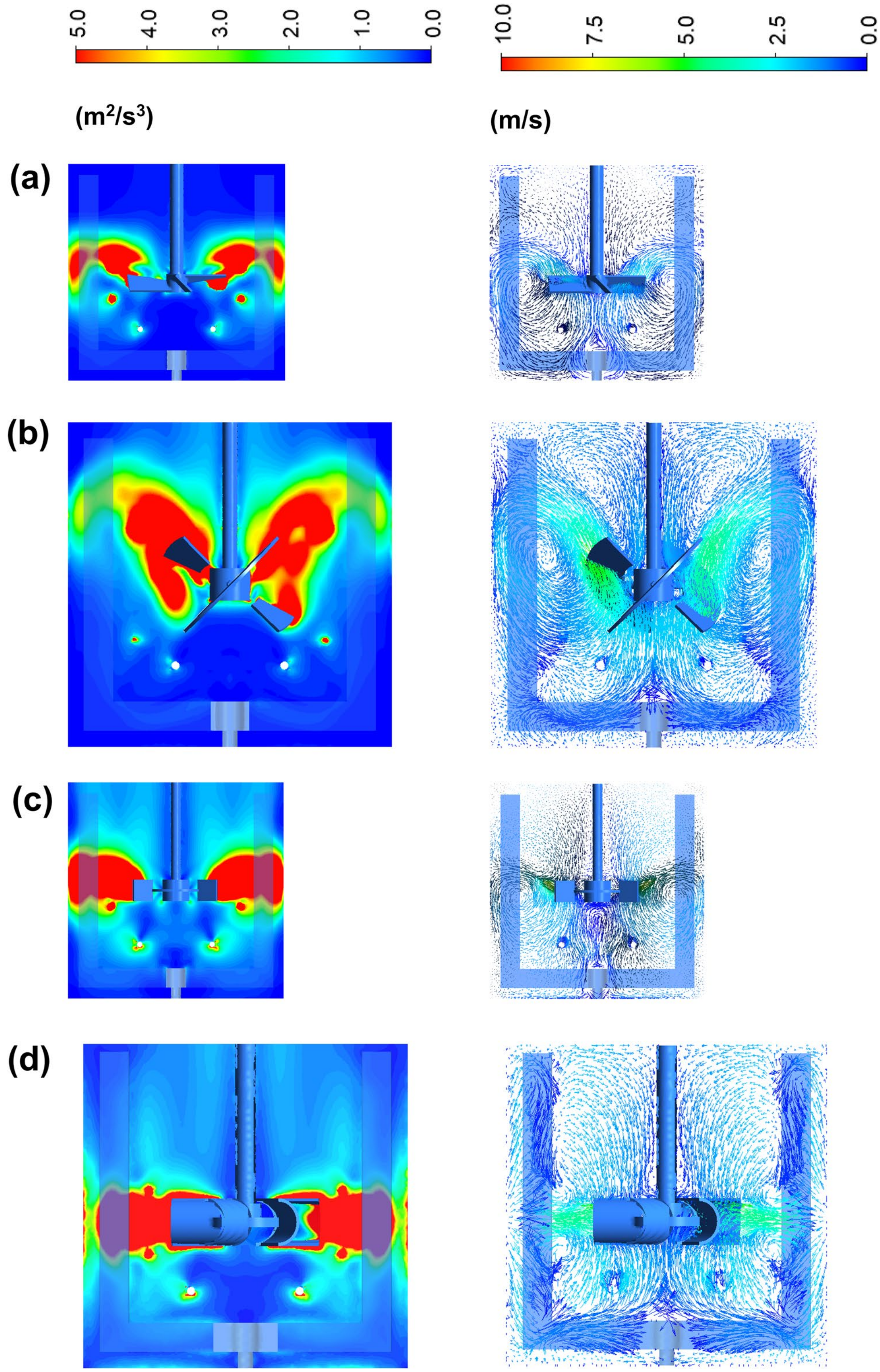

Fig. 9 CFD outcomes pertaining to the fluid velocity vector and the rate of energy dissipation in the coaxial bioreactor during the scale-up process via central impeller retrofitting (for all cases, aeration rate = 0.20 vvm): **a** Pitched blade-anchor, **b** Elephant ear-anchor, **c** Rushton turbine-anchor, and **d** Scaba-anchor

shear environment compared to the axial-flow impeller. The shear environment of the system increased during the scale-up, because large-scale mixers required more power to keep the mass transfer rate constant. However, the scale-up study incorporating central impeller retrofitting demonstrated a promising approach for optimizing large-scale processes, achieving high mass transfer while reducing the shear environment.

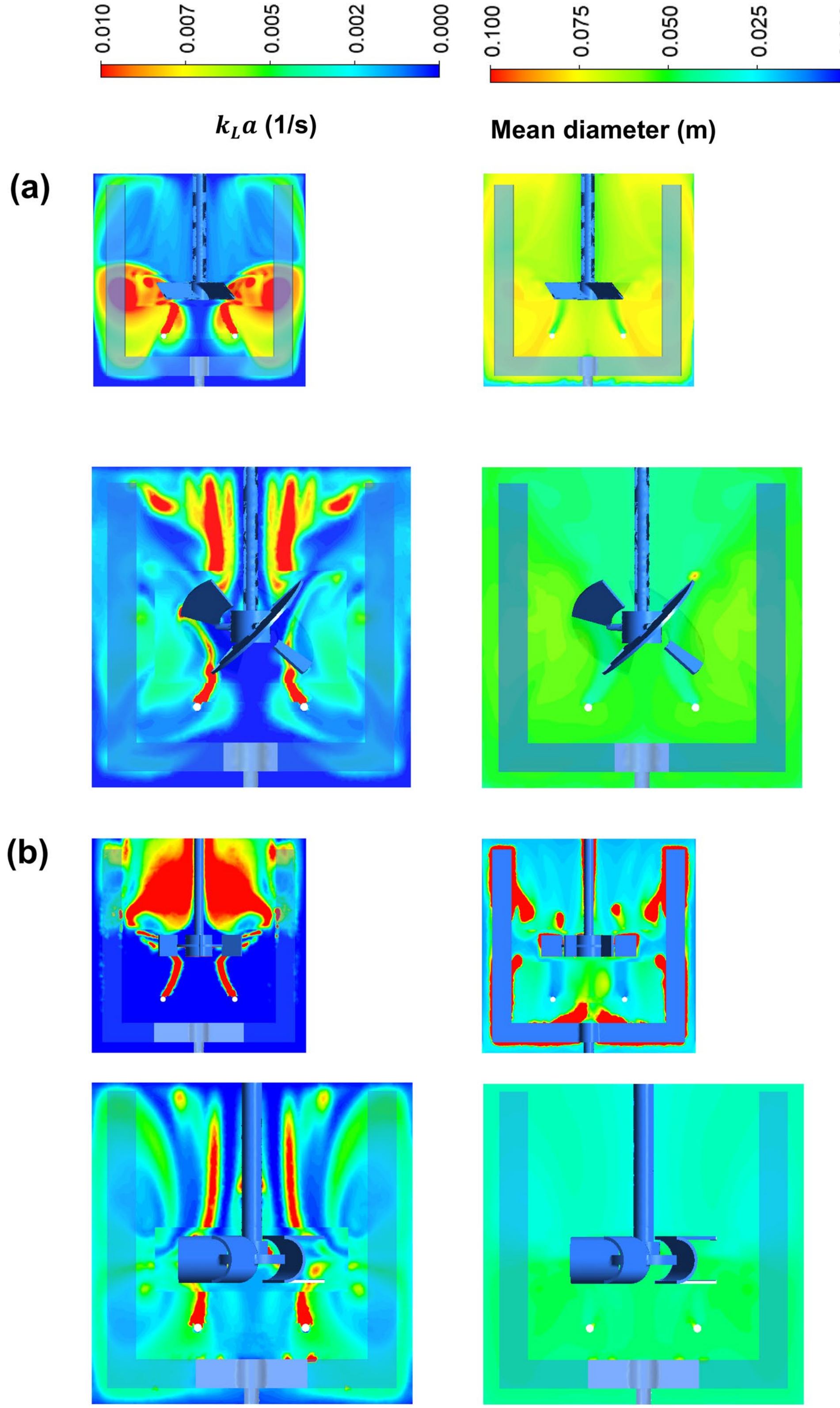

Fig. 10 CFD outcomes pertaining to the mean diameter of air bubbles and k_La in the coaxial bioreactor during the scale-up process via central impeller retrofitting: **a** bioreactor furnished with an axial-flow impeller, and **b** bioreactor furnished with a radial-flow impeller

Acknowledgements Computations were performed on the Niagara supercomputer at the SciNet HPC Consortium. The authors are deeply grateful to ANSYS for providing us with a high-performance computing license for the ANSYS FLUENT software.

Author contributions AR: Conceptualization, Methodology, Software, Model Development & Validation, Data Analysis, Writing – Original DraftFE: Conceptualization, Resources, Methodology, Writing – Review & Editing, Supervision, Project Administration, Funding AcquisitionAL: Conceptualization, Resources, Methodology, Writing – Review & Editing, Supervision, Project Administration, Funding Acquisition

Funding The financial support of the Natural Sciences and Engineering Research Council of Canada (NSERC: RGPIN-2019–04644) is gratefully acknowledged.

Declarations

Conflict of interests The authors declare no competing interests.

References

1. Amanullah A, Blair R, Nienow AW, Thomas CR (1999) Effects of agitation intensity on mycelial morphology and protein production in chemostat cultures of recombinant aspergillus oryzae. Biotechnol Bioeng 62:434–446. https://doi.org/10.1002/(SICI)1097-0290(19990220)62:4%3c434::AID-BIT6%3e3.0.CO;2-D
2. Amanullah A, Jüsten P, Davies A, Paul GC, Nienow AW, Thomas CR (2000) Agitation induced mycelial fragmentation of Aspergillus oryzae and Penicillium chrysogenum. Biochem Eng J 5:109–114. https://doi.org/10.1016/S1369-703X(99)00059-5
3. Dreher T, Husemann U, Adams T, de Wilde D (2000) Design space definition for a stirred single-use bioreactor family from 50 to 2000 L scale. Eng Life Sci 14(2014):304–310. https://doi.org/10.1002/elsc.201300067
4. Nienow AW (2021) The impact of fluid dynamic stress in stirred bioreactors – the scale of the biological entity: a personal view. Chemie Ing Tech 93:17–30. https://doi.org/10.1002/cite.202000176
5. Schlaich EM, Thomas JA, Kandari L, Tremml G, Khetan A (2023) Experimental and computational characterization of mass transfer in high turndown bioreactors. Biotechnol Prog 1:1–13. https://doi.org/10.1002/btpr.3330
6. Abu-Reesh I, Kargi F (1991) Biological responses of hybridoma cells to hydrodynamic shear in an agitated bioreactor. Enzyme Microb Technol 13:913–919. https://doi.org/10.1016/0141-0229(91)90108-M
7. Villiger TK, Neunstoecklin B, Karst DJ, Lucas E, Stettler M, Broly H, Morbidelli M, Soos M (2018) Experimental and CFD physical characterization of animal cell bioreactors: From micro- to production scale. Biochem Eng J 131:84–94. https://doi.org/10.1016/j.bej.2017.12.004
8. Oh SKW, Nienow AW, Al-Rubeai M, Emery AN (1989) The effects of agitation intensity with and without continuous sparging on the growth and antibody production of hybridoma cells. J Biotechnol 12:45–61. https://doi.org/10.1016/0168-1656(89)90128-4
9. Buffo MM, Corrêa LJ, Esperança MN, Cruz AJG, Farinas CS, Badino AC (2016) Influence of dual-impeller type and configuration on oxygen transfer, power consumption, and shear rate in a stirred tank bioreactor. Biochem Eng J 114:130–139. https://doi.org/10.1016/j.bej.2016.07.003
10. Nienow AW (2009) Scale-up considerations based on studies at the bench scale in stirred bioreactors. J Chem Eng Japan 42:789–796. https://doi.org/10.1252/jcej.08we317
11. Maluta F, Alberini F, Montante G, Paglianti A (2022) Validation of a procedure for the numerical simulations of gas–liquid stirred tanks by means of a computational fluid dynamics approach. Can J Chem Eng 100:3472–3485. https://doi.org/10.1002/cjce.24548
12. Bach C, Yang J, Larsson H, Stocks SM, Gernaey KV, Albaek MO, Krühne U (2017) Evaluation of mixing and mass transfer in a stirred pilot scale bioreactor utilizing CFD. Chem Eng Sci 171:19–26. https://doi.org/10.1016/j.ces.2017.05.001
13. Zheng JL, Shukla V, Wenger KS, Fordyce AP, Pedersen AG, Marten MR (2002) Effects of increased impeller power in a production-scale Aspergillus oryzae fermentation. Biotechnol Prog 18:437–444. https://doi.org/10.1021/bp020023c
14. Esperança MN, Buffo MM, Mendes CE, Rodriguez GY, Béttega R, Badino AC, Cerri MO (2022) Linking maximal shear rate and energy dissipation/circulation function in airlift bioreactors. Biochem Eng J. https://doi.org/10.1016/j.bej.2021.108308
15. Nienow AW (2010) Scale-up, stirred tank reactors. Encycl Ind Biotechnol. https://doi.org/10.1002/9780470054581.eib535
16. Sieck JB, Cordes T, Budach WE, Rhiel MH, Suemeghy Z, Leist C, Villiger TK, Morbidelli M, Soos M (2013) Development of a Scale-Down Model of hydrodynamic stress to study the performance of an industrial CHO cell line under simulated production scale bioreactor conditions. J Biotechnol 164:41–49. https://doi.org/10.1016/j.jbiotec.2012.11.012
17. Scully J, Considine LB, Smith MT, McAlea E, Jones N, O'Connell E, Madsen E, Power M, Mellors P, Crowley J, O'Leary N, Carver S, Van Plew D (2020) Beyond heuristics: CFD-based novel multiparameter scale-up for geometrically disparate bioreactors demonstrated at industrial 2kL–10kL scales. Biotechnol Bioeng 117:1710–1723. https://doi.org/10.1002/bit.27323
18. Takors R (2012) Scale-up of microbial processes: Impacts, tools and open questions. J Biotechnol 160:3–9. https://doi.org/10.1016/j.jbiotec.2011.12.010
19. Gelves R, Dietrich A, Takors R (2014) Modeling of gas-liquid mass transfer in a stirred tank bioreactor agitated by a Rushton turbine or a new pitched blade impeller. Bioprocess Biosyst Eng 37:365–375. https://doi.org/10.1007/s00449-013-1001-8
20. Cappello V, Plais C, Vial C, Augier F (2021) Scale-up of aerated bioreactors: CFD validation and application to the enzyme production by Trichoderma reesei. Chem Eng Sci 229:116033. https://doi.org/10.1016/j.ces.2020.116033
21. Nienow AW (2006) Reactor engineering in large scale animal cell culture. Cytotechnology 50:9–33. https://doi.org/10.1007/s10616-006-9005-8
22. Maluta F, Pigou M, Montante G, Morchain J (2020) Modeling the effects of substrate fluctuations on the maintenance rate in bioreactors with a probabilistic approach. Biochem Eng J. https://doi.org/10.1016/j.bej.2020.107536
23. Liu E, Wilkins MR (2020) Process optimization and scale-up production of fungal aryl alcohol oxidase from genetically modified Aspergillus nidulans in stirred-tank bioreactor. Bioresour Technol 315:123792. https://doi.org/10.1016/j.biortech.2020.123792
24. Kazemzadeh A, Elias C, Tamer M, Ein-Mozaffari F (2018) Hydrodynamic performance of a single-use aerated stirred bioreactor in animal cell culture: applications of tomography, dynamic gas disengagement (DGD), and CFD. Bioprocess Biosyst Eng 41:679–695. https://doi.org/10.1007/s00449-018-1902-7
25. Zhao X, Ren L, Guo D, Wu W, Ji X, Huang H (2016) CFD investigation of Schizochytrium sp. impeller configurations on cell

growth and docosahexaenoic acid synthesis. Bioprocess Biosyst Eng 39:1297–1304. https://doi.org/10.1007/s00449-016-1608-7
26. Nienow AW, Hunt G, Buckland BC (1994) A fluid dynamic study of the retrofitting of large agitated bioreactors: turbulent flow. Biotechnol Bioeng 44:1177–1185. https://doi.org/10.1002/bit.260441004
27. Hardy N, Augier F, Nienow AW, Béal C, Ben-Chaabane F (2017) Scale-up agitation criteria for Trichoderma reesei fermentation. Chem Eng Sci 172:158–168. https://doi.org/10.1016/j.ces.2017.06.034
28. Jüsten P, Paul GC, Nienow AW, Thomas CR (1996) Dependence of mycelial morphology on impeller type and agitation intensity. Biotechnol Bioeng 52:672–684. https://doi.org/10.1002/(SICI)1097-0290(19961220)52:6%3c672::AID-BIT5%3e3.0.CO;2-L
29. Maltby R, Tian S, Chew YMJ (2018) Computational studies of a novel magnetically driven single-use-technology bioreactor: a comparison of mass transfer models. Chem Eng Sci 187:157–173. https://doi.org/10.1016/j.ces.2018.05.006
30. Ding J, Wang X, Zhou XF, Ren NQ, Guo WQ (2010) CFD optimization of continuous stirred-tank (CSTR) reactor for biohydrogen production. Bioresour Technol 101:7005–7013. https://doi.org/10.1016/j.biortech.2010.03.146
31. Cheung CKL, Leksawasdi N, Doran PM (2018) Bioreactor scale-down studies of suspended plant cell cultures. AIChE J 64:4281–4288. https://doi.org/10.1002/aic.16415
32. Zou X, Xia JY, Chu J, Zhuang YP, Zhang SL (2012) Real-time fluid dynamics investigation and physiological response for erythromycin fermentation scale-up from 50 L to 132 m 3 fermenter. Bioprocess Biosyst Eng 35:789–800. https://doi.org/10.1007/s00449-011-0659-z
33. Rathore AS, Sharma C, Persad A (2012) Use of computational fluid dynamics as a tool for establishing process design space for mixing in a bioreactor. Biotechnol Prog 28:382–391. https://doi.org/10.1002/btpr.745
34. Sharifi F, Behzadfar E, Ein-mozaffari F (2023) Intensified gas-liquid mixing in bioreactors equipped with a dual coaxial mixer containing biopolymer solutions. Chem Eng Res Des 191:109–126. https://doi.org/10.1016/j.cherd.2023.01.026
35. Barros PL, Ein-Mozaffari F, Lohi A (2022) Power Consumption Characterization of Energy-Efficient Aerated Coaxial Mixers Containing Yield-Stress Biopolymer Solutions. Ind Eng Chem Res 61:12813–12824. https://doi.org/10.1021/acs.iecr.2c02008
36. Rahimzadeh A, Ein-mozaffari F, Lohi A (2023). A Methodical Approach to Scaling Up an Aerated Coaxial Mixer Containing a Shear-Thinning Fluid : Effect of the Fluid Rheology. https://doi.org/10.1021/acs.iecr.3c00464
37. Rahimzadeh A, Ein-mozaffari F, Lohi A (2023) Development of a scale-up strategy for an aerated coaxial mixer containing a non-Newtonian fluid: a mass transfer approach. Phys Fluids. https://doi.org/10.1063/5.0155777
38. Rahimzadeh A, Ein-mozaffari F, Lohi A (2022) Investigation of power consumption, torque fluctuation, and local gas hold-up in coaxial mixers containing a shear-thinning fluid : experimental and numerical approaches. Chem Eng Process - Process Intensif 177:108983. https://doi.org/10.1016/j.cep.2022.108983
39. Nienow AW, Hunt G, Buckland BC (1996) A fluid dynamic study using a simulated viscous, shear thinning broth of the retrofitting of large agitated bioreactors. Biotechnol Bioeng 49:15–19. https://doi.org/10.1002/(SICI)1097-0290(19960105)49:1%3c15::AID-BIT2%3e3.0.CO;2-W
40. Morchain J, Gabelle J-C, Cockx A (2014) A coupled population balance model and CFD approach for the simulation of mixing issues in lab-scale and industrial bioreactors. AIChE J 60:27–40. https://doi.org/10.1002/aic.14238
41. Mohd-Sauid S, Krishnan J, Huey-Ling T, Veluri MVPS (2013) Enhancement of oxygen mass transfer and gas holdup using palm oil in stirred tank bioreactors with xanthan solutions as simulated viscous fermentation broths. Biomed Res Int. https://doi.org/10.1155/2013/409675
42. Sadino-Riquelme MC, Rivas J, Jeison D, Donoso-Bravo A, Hayes RE (2022) Investigating a stirred bioreactor: impact of evolving fermentation broth pseudoplastic rheology on mixing mechanisms. Fermentation 8:1. https://doi.org/10.3390/fermentation8030102
43. Núñez-Ramírez DM, Valencia-López JJ, Calderas F, Solís-Soto A, López-Miranda J, Medrano-Roldán H, Medina-Torres L (2012) Mixing analysis for a fermentation broth of the fungus beauveria bassiana under different hydrodynamic conditions in a bioreactor. Chem Eng Technol 35:1954–1961. https://doi.org/10.1002/ceat.201200130
44. Caşcaval D, Galaction AI, Turnea M (2011) Comparative analysis of oxygen transfer rate distribution in stirred bioreactor for simulated and real fermentation broths. J Ind Microbiol Biotechnol 38:1449–1466. https://doi.org/10.1007/s10295-010-0930-3
45. J.-C. Gabelle, J. Morchain, D. Anne-Archard, F. Augier, A. Liné, Experimental determination of the shear rate in a stirred tank with a non-newtonian fluid: Carbopol, AIChE J. 59 (2013) 2251–2266. https://doi.org/10.1002/aic.13973.
46. Li X, Scott K, Kelly WJ, Huang Z (2018) Development of a computational fluid dynamics model for scaling-up ambr bioreactors. Biotechnol Bioprocess Eng 23:710–725. https://doi.org/10.1007/s12257-018-0063-5
47. Sato Y, Sekoguchi K (1975) Liquid velocity distribution in two-phase bubble flow. Int J Multiph Flow 2:79–95. https://doi.org/10.1016/0301-9322(75)90030-0
48. Brucato A, Grisafi F, Montante G (1998) Particle drag coefficients in turbulent fluids. Chem Eng Sci 53:3295–3314. https://doi.org/10.1016/S0009-2509(98)00114-6
49. Laakkonen M, Moilanen P, Miettinen T, Saari K, Honkanen M, Saarenrinne P, Aittamaa J (2005) Local bubble size distributions in agitated vessel comparison of three experimental techniques. Chem Eng Res Des 83:50–58. https://doi.org/10.1205/cherd.04122
50. H. Luo, Coalescence, breakup and liquid circulation in bubble column reactors (1995).
51. Higbie R (1935) The rate of absorption of a pure gas into a still liquid during short periods of exposure. Trans AIChE 31:365–389
52. Ebrahimi M, Tamer M, Villegas RM, Chiappetta A, Ein-Mozaffari F (2019) Application of CFD to analyze the hydrodynamic behaviour of a bioreactor with a double impeller. Processes. https://doi.org/10.3390/pr7100694
53. Roussinova V, Kresta SM, Weetman R (2003) Low frequency macroinstabilities in a stirred tank: scale-up and prediction based on large eddy simulations. Chem Eng Sci 58:2297–2311. https://doi.org/10.1016/S0009-2509(03)00097-6
54. Miller DN (1974) Scale-up of agitated vessels gas-liquid mass transfer. AIChE J 20:445–453